RESEARCH ARTICLE

Macromolecular Rapid Communications
www.mrc-journal.de

Achieving High Performance Stretchable Conjugated Polymers via Donor Structure Engineering

Ning Wu, Gang Huang, Hua Huang, Yunfei Wang, Xiaodan Gu, Xiaohong Wang, and Longzhen Qiu**

A backbone engineering strategy is developed to tune the mechanical and electrical properties of conjugated polymer semiconductors. Four Donor–Acceptor (D–A) polymers, named PTDPPSe, PTDPPTT, PTDPPBT, and PTDPPTVT, are synthesized using selenophene (Se), thienothiophene (TT), bithiophene (BT), and thienylenevinylenethiophene (TVT) as the donors and siloxane side chain modified diketopyrrolopyrrole (DPP) as acceptor. The influences of the donor structure on the polymer energy level, film morphology, molecular stacking, carrier transport properties, and tensile properties are all examined. The films of PTDPPSe show the best stretchability with crack-onset-strain greater than 100%, but the worst electrical properties with a mobility of only 0.54 $cm^2 V^{-1} s^{-1}$. The replacement of the Se donor with larger conjugated donors, that is, TT, BT, and TVT, significantly improves the mobility of conjugated polymers but also leads to reduced stretchability. Remarkably, PTDPPBT exhibits moderate stretchability with crack-onset-strain ≈50% and excellent electrical properties. At 50% strain, it has a mobility of 2.37 $cm^2 V^{-1} s^{-1}$ parallel to the stretched direction, which is higher than the mobility of most stretchable conjugated polymers in this stretching state.

1. Introduction

With the increasing demand for embeddable, portable, highly sensitive, and real-time monitoring medical devices, stretchable electronic components have attracted particular interest for application in such devices.[1–3] Conjugated polymers have emerged as the next generation of semiconductor layer materials for stretchable electronic components, among which donor–acceptor (D–A) conjugated polymers have received special attention due to their efficient carrier mobility.[4–6] However, the backbone of D–A conjugated polymers are mainly composed of aromatic rings, which are highly rigid and semicrystalline, and thus are unfavorable for the mechanical ductility of the films.[7] Their stretchability has been further enhanced through molecular design,[8–10] geometric engineering, and physical blending strategies to achieve harmonious human-computer interactions.[11–15] Nevertheless, the complex process of geometric engineering and inferior mobility of the non-conjugated materials used in blending methods leads to the molecular design strategy being more competitive. Molecular design strategies are advantageous in terms of substantial tunability. The superiorly stretchable conjugated polymer can be obtained by combining with backbone engineering,[16–19] side chain engineering,[20–22] and molecular weight controlling.[23,24]

In the design and synthesis of intrinsically stretchable D–A polymer structures, the acceptor unit is usually investigated by introducing solubilizing side chains, as well as dynamic bonding units containing hydrogen bonds, and other functional side chains, such as biaxially extended conjugated side chain and oligosiloxane side chain.[25–28] On the other hand, the donor unit also controlled the conformation of the polymer and adjusted the stretchability of the film by tuning the number of rigid fused rings, or inserting free flexible nonconjugated spacers in the donor, and introducing side chains in the rigid fused rings of the donor.[29–31] For instance, Gu et al. investigated the effect of thiophene ring structure on the glass transition temperature and film modulus of polymers using thiophene (T), bithiophene (T2), terthiophene (T3), thienothiophene (TT), and dithienothiophene (TTT) as the donor. The best tensile properties of the polymers were found with thiophene as donors.[29] The conclusions from the research indicate that the donor structure plays an important role in modulating the electrical and mechanical properties of D–A conjugated polymers. By embedding different flexible conjugate fracture linkage bonds in the donor unit, Bao et al. revealed

N. Wu, G. Huang, H. Huang, X. Wang, L. Qiu
National Engineering Lab of Special Display Technology
Special Display and Imaging Technology Innovation Center of Anhui Province
Academy of Opto-Electronic Technology
Hefei University of Technology
Hefei 230009, China
E-mail: xhwang11@hfut.edu.cn; lzhqiu@hfut.edu.cn

N. Wu, G. Huang, H. Huang, X. Wang, L. Qiu
Intelligent Interconnected Systems Laboratory of Anhui
Anhui Province Key Laboratory of Measuring Theory and Precision Instrument
School of Instrument Science and Opto-Electronic Engineering
Hefei University of Technology
Hefei 230009, China

Y. Wang, X. Gu
School of Polymer Science and Engineering
The University of Southern Mississippi
Hattiesburg, MS 39406, USA

The ORCID identification number(s) for the author(s) of this article can be found under https://doi.org/10.1002/marc.202300169

DOI: 10.1002/marc.202300169

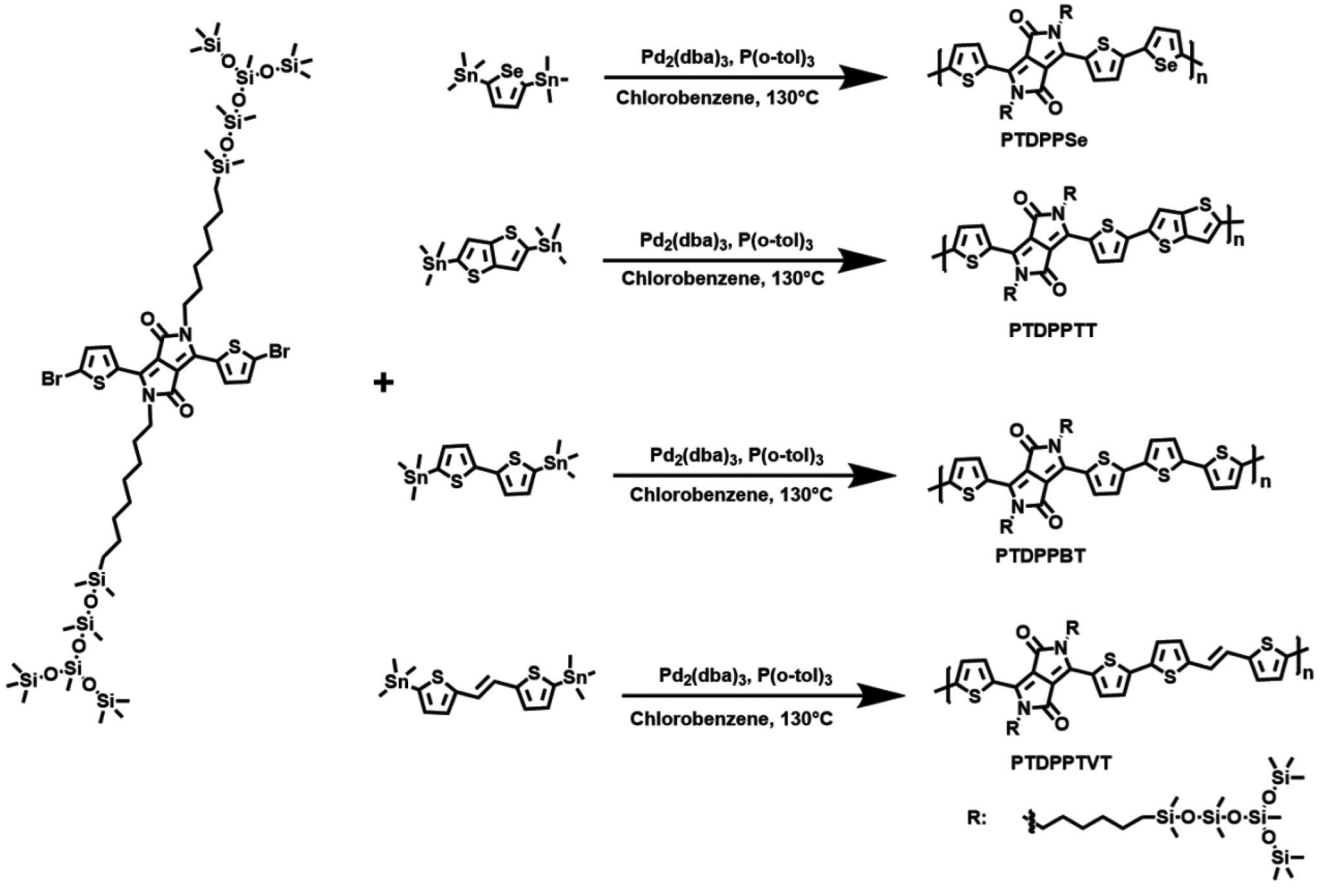

Scheme 1. Synthetic routes of polymers PTDPPSe, PTDPPTT, PTDPPBT, and PTDPPTVT.

that adding a conjugate disruptor at 10 mol % improved the crack onset strain and modulus at the expense of only a modest decrease in mobility.[31] However, the low flexibility of the alkyl side chains caused the polymer mobility to be lower than the unstretched state at high strains in all of the above studies. Such a phenomenon may limit the widespread application of the donor structure in the property modulation of D–A conjugated polymers. In our recent work, by replacing the alkyl side chain with a bulky siloxane side chain, it was found that the obtained conjugated polymers showed obvious strain-induced molecular chain alignment and their electrical properties increase with increasing the stretching ratio.[19,22] However, the large volume of the siloxane side chains results in low mobility of the polymer in the unstretched state. Therefore, we hope to improve the carrier transport properties of the polymer while maintaining excellent stretchability through backbone designs.

In this study, D–A polymers were designed and prepared in which siloxane-modified diketopyrrolopyrrole (DPP) was selected as the acceptor, and selenophene (Se), thienothiophene (TT), bithiophene (BT), and thienylenevinylenethiophene (TVT) as donors to yield polymers, PTDPPSe, PTDPPTT, PTDPPBT, and PTDPPTVT, respectively. The optical properties, microstructures, and electrical and mechanical properties of all four D–A polymers were characterized by various analytical methods. Atomic force microscopy (AFM) and optical microscopy (OM) were employed to study the microscopic morphology of resulting polymer films. The grazing-incidence wide-angle X-ray scattering (GIWAXS) was utilized for the characterization of the orientation state of polymer molecular chains.[32] Field-effect performance was used for the measurement of the carrier transport efficiency of the four polymers at different temperatures and strains. The experimental results revealed a direct effect of the donor structure on the backbone stacking and film morphology of the polymer. Thus, an optimal donor-acceptor combination was determined to yield D–A conjugated polymers with high electrical and mechanical properties.

2. Results and Discussion

2.1. Synthesis of Polymers

The siloxane-modified DPP-based copolymers were prepared by the synthetic procedure outlined in **Scheme 1** and Supporting Information (SI).^{1}H NMR spectra were used to determine the correctness of the individual step monomers. The purchased silicon chains (H-3Si) were subjected to a multi-step reaction to extend the length of the silicon side chain to H-5Si. The DPP was selected as the backbone acceptor unit due to its favorable charge transport properties and chemical stability. Then Stille coupling was performed on the brominated DPP acceptor and the four

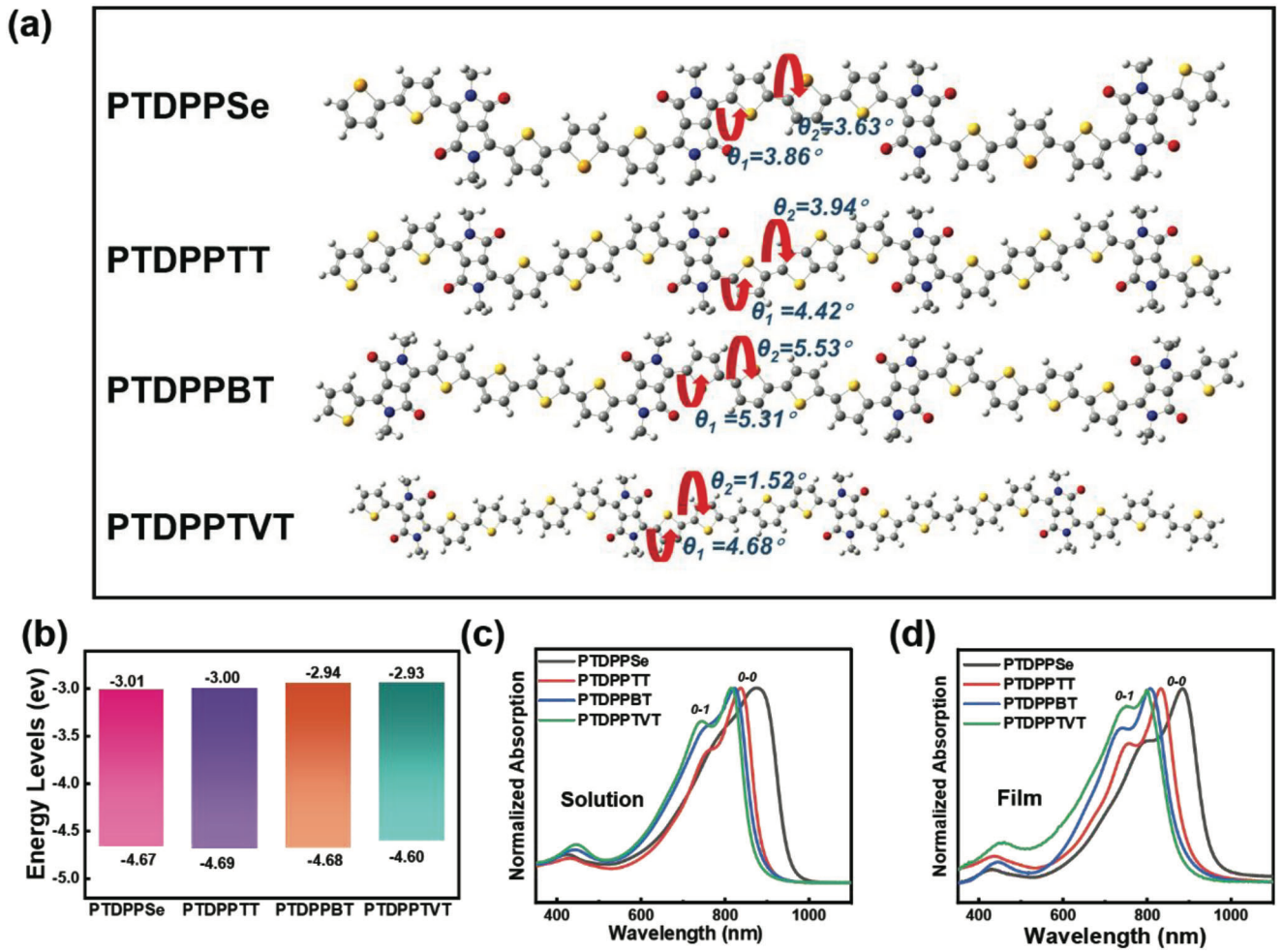

Figure 1. a) Optimized geometries of PTDPPSe, PTDPPTT, PTDPPBT, and PTDPPTVT tetramer computed using the B3LYP/6-31 (d) model. b) Frontier orbital distributions of methyl-substituted tetramer obtained by DFT calculations. c,d) UV–vis absorption spectra of polymers in chloroform (c) and as a film (d).

donors with uniform polymerization time, temperature, and 1:1 ratio of donor to acceptor. After Soxhlet extraction, the expected polymer was achieved. The M_n values of PTDPPSe, PTDPPTT, PTDPPBT, and PTDPPTVT were recorded as 327, 372, 289, and 380 kDa, while the corresponding PDI values were estimated to be 1.90, 1.87, 1.95, and 1.77, respectively. The high molecular weights were attributed to the good solubility of the acceptor unit, which would be favorable for stretchability properties.

2.2. Density Functional Theory Calculations

To gain further insights into the effect of the donor structure on the electron cloud distribution and chain conformation of the frontier orbitals of the polymer molecules, the density functional theory (DFT) calculations were performed for the series polymers using the B3LYP/6-31 (d) model, simplified by replacing the siloxane side chain on the DPP acceptor with a methyl group (**Figure 1**a). The molecular structures of the polymers constructed from the four different donors were compared, and the results revealed HOMO and LUMO energy levels ≈−2.9 and −4.7 eV for the four polymers, exhibiting a narrow energy band gap (Figure 1b). The four different model molecules' front-line molecular orbitals were distributed along the entire conjugated backbone at both the HOMO and LUMO energy levels (E_{HOMO} and E_{LUMO}). The simulation results of the two angles of the conjugated backbone were shown in Figure 1a. Note that the plane angle between the DPP group and the flanking group was denoted as θ_1, while the torsion angle between the acceptor and the donor was θ_2. The angles θ_1 for the four polymers ranged from 3.68° to 5.31°. The similar θ_1 values originated from the hydrogen bonding formed between adjacent O···H atoms in the DPP acceptor, which can produce conformational locking.[33] Among the four polymers, PTDPPBT displayed the largest torsion angle θ_2, attributed to the flexibility of the bithiophene donor. On the other hand, the large torsion angle θ_2 reduced the stacking density of the conjugated backbone, which is probably favorable for enhanced tensile properties of the polymer. The tetrameric molecular simulations of PTDPPSe and PTDPPTVT exhibited high planarity. However, the much higher side chain density of polymer PTDPPSe than that of PTDPPTVT may indicate inferior actual crystallinity of PTDPPSe than that of polymer PTDPPTVT (the

Table 1. The optical and electrochemical properties of four polymers were obtained with different donor units.

Polymer	M_n[kDa]	M_w[kDa]	PDI	λ_{max}^{solu}[nm]	λ_{max}^{film} [nm]	E_g^{opt}[ev][a)]
PTDPPSe	327	623	1.90	881	882	1.31
PTDPPTT	372	696	1.87	838	833	1.40
PTDPPBT	289	561	1.95	823	808	1.41
PTDPPTVT	380	674	1.77	816	800	1.43

[a)] $E_g^{opt} = 1240/\lambda_{onset}$ (denotes films annealed at 25 °C).

calculation results for the four monomer lengths were shown in Table S4, Supporting Information).

2.3. Absorption Spectra and Frontier Orbital Energy Levels

To investigate the effects of donor structure on the aggregation state of D–A molecules, UV–vis absorption spectroscopy of four polymers was recorded in chloroform solution and spin-coated films (Figure 1c,d), and detailed data are summarized in **Table 1**. As shown in Figure 1c,d, the positions of the maximum absorption peaks (λ_{max}) of each polymer solution gradually blue-shifted, with λ_{max} ranging from 881 nm for PTDPPSe to 816 nm for PTDPPTVT. Hence, the conjugate length of the molecular chains was effectively affected by the donor's structures.[34] The spectra of PTDPPTT, PTDPPBT, and PTDPPTVT exhibited distinct 0-0 and 0–1 peaks in chloroform solution, with PTDPPTT showing the largest 0-0/0-1 values. This phenomenon suggests PTDPPTT exhibited the strongest pre-aggregation in chloroform solution. Similar to the solution absorption, the λ_{max} values of the four polymers in the thin film state gradually blue-shifted for PTDPPSe, PTDPPTT, PTDPPBT, and PTDPPTVT. All four polymers exhibited narrow optical band gaps with E_g^{opt} estimated to 1.31 eV for PTDPPSe, 1.40 eV for PTDPPTT, 1.41 eV for PTDPPBT, and 1.43 eV for PTDPPTVT.

The frontier orbital energy levels of four polymers PTDPPSe, PTDPPTT, PTDPPBT, and PTDPPTVT were evaluated by cyclic voltammetry (CV), and the results are provided in Figure S1 (Supporting Information). The E_{HOMO} and E_{LUMO} values obtained by the CV method were −3.35 and −5.07 eV for PTDPPSe, −3.32 and −5.02 eV for PTDPPTT, −3.36 and −5.01 eV for PTDPPBT, and −3.33 and −4.96 eV for PTDPPTVT. These data results agreed well with the values from DFT simulations.[35]

2.4. Micromorphology and Molecular Stacking of Polymer Films

AFM studied the effect of donor structure on film morphology at the macroscopic level. To this end, films of PTDPPSe, PTDPPTT, PTDPPBT, and PTDPPTVT were obtained by spin-coating chloroform solutions onto CYTOP-modified SiO_2/Si substrates. As shown in Figure S4 (Supporting Information), the as-cast film of PTDPPSe had the smallest root-mean-square roughness (RMS) value of 1.48 nm among the four polymers. By comparison, the as-cast films of PTDPPTT, PTDPPBT, and PTDPPTVT showed more obvious nanowire-like structures, with RMS higher than that of PTDPPSe. Compared to the as-cast films, the four annealed polymer films displayed rougher surface morphologies due to the enhanced film crystallization caused by the rearrangement of polymer molecular chains promoted by annealing. Remarkably, annealed films of PTDPPTT, PTDPPBT, and PTDPPTVT presented apparent holes.[36] This phenomenon may be attributed to the high planarity of the molecular backbone combined with less entanglement of the molecular chains of the three polymers, which makes the molecular chain of PTDPPTT, PTDPPBT, and PTDPPTVT more prone to long-distance movement with the increase of temperature.

To investigate the effects of donor structures on the crystallinity and molecular stacking of conjugated polymers, GIWAXS was performed on polymer films before and after annealing.[37–40] As presented in **Figure 2**a,b, all polymer films illustrated clear lamellar diffraction peaks. The diffraction peaks in the out-of-plane direction (*h*00) became sharper for four polymers after annealing, indicating a more ordered stacking of molecules after annealing caused by the rearrangement of polymer chain segments. PTDPPSe showed (010) diffraction peak in the out-of-plane direction which indicates the backbones of PTDPPSe adopt face-on orientation in both as-cast and annealed films. However, PTDPPTT, PTDPPBT, and PTDPPTVT exhibited shaper (*h*00) diffraction peaks along the out-of-plane direction and (010) diffraction peaks along the in-plane direction indicating they are mainly edge-on alignments. Among all four polymers, PTDPPSe exhibited the largest lamellar spacing (31.34 Å), and π-π stacking distance (3.77 Å) (Figure 2c, Table S1, Supporting Information) due to its highest side chain density. While the PTDPPTVT depicted the smallest lamellar spacing (29.06 Å), π–π stacking distance (3.53 Å). The coherence length values for PTDPPTT, PTDPPBT, and PTDPPTVT are 197.17, 134.62, and 163.11 Å, respectively, which are significantly greater than the coherence length values for PTDPPSe (117.05 Å). These results indicate that donor structure has an important influence on the arrangement of polymer chains, which further affects their electrical and mechanical properties.

2.5. OFET Performance of Polymer Films

To explore the effects of the donor structures on the charge transport properties of the polymers, a series of bottom-gate-top-contact (BGTC) structured field-effect transistors (OFETs) were prepared, and the device preparation details were provided in the Experimental Section. After spin coating of the prepared solutions, all films were annealed under a nitrogen atmosphere at different temperatures. Table S2 (Supporting Information) summarizes the max and average mobility of all films of the devices at different temperatures, and **Figure 3**a depicts the transfer curves for the devices at room temperature. All polymers exhibited typical p-type field effect properties. The average carrier mobilities at room temperature of PTDPPSe, PTDPPTT, PTDPPBT, and PTDPPTVT were estimated to be 0.54, 0.93, 1.24, and 1.27 $cm^2\ V^{-1}\ s^{-1}$, respectively. The corresponding max mobility values were 0.58, 1.05, 1.32, and 1.33 $cm^2\ V^{-1}\ s^{-1}$, respectively. PTDPPSe showed the lowest electrical properties since its poor crystallinity is harmful to carrier transport. The highest side chain density of PTDPPSe leads to poor crystallinity and maximum π–π stacking distances, resulting in difficult carrier hopping between molecular chains and poor electrical properties. By

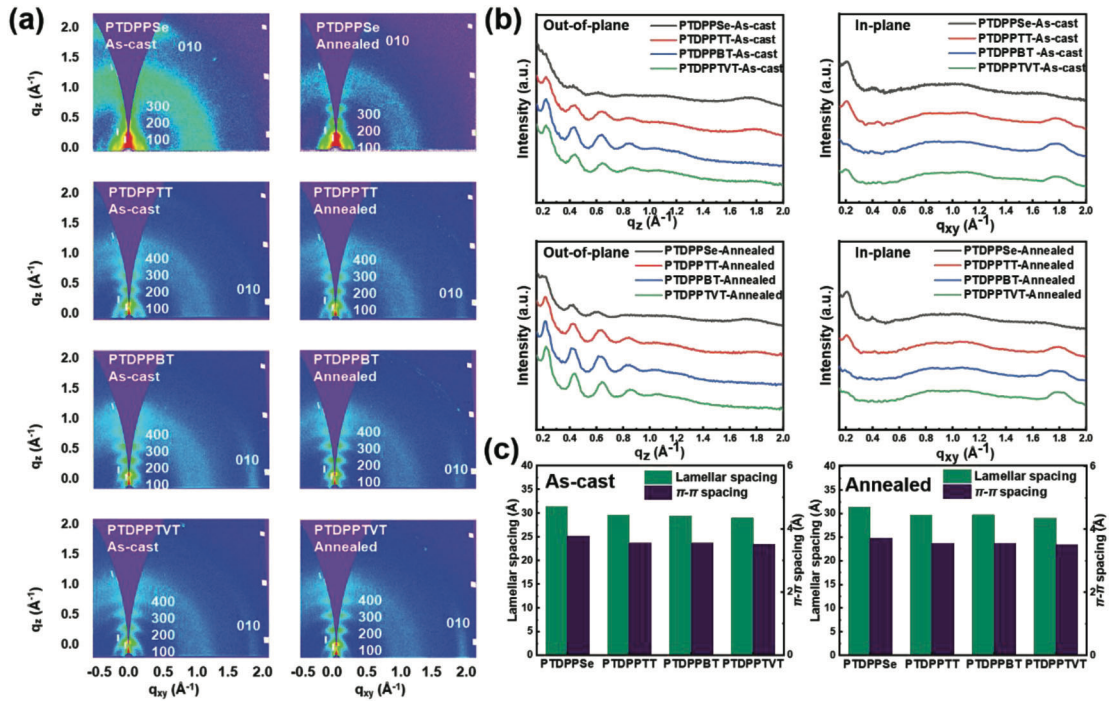

Figure 2. a) 2D GIWAXS data of four polymer films before and after annealing at 180 °C. b) 1D GIWAXS data of four polymer films before and after annealing at 180 °C. c) Lamellar spacing and π–π spacing of the four polymer films as cast and annealed.

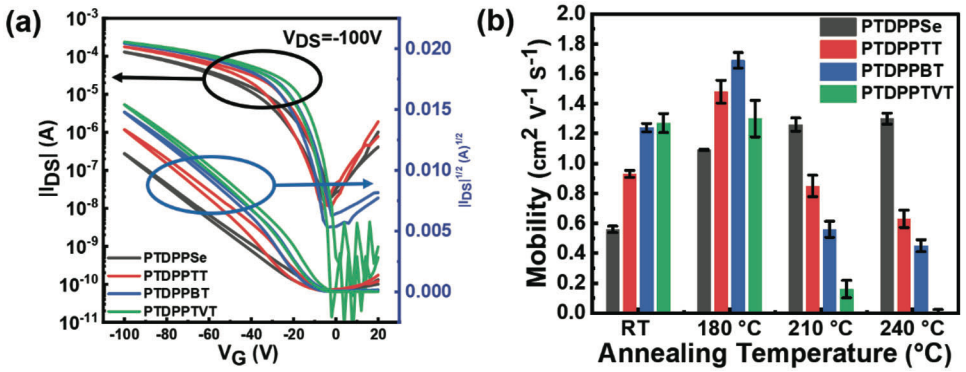

Figure 3. a) Transfer curves of the four polymers at room temperature. b) Histogram of the mobility of the four polymers at different annealing temperatures (RT (25 °C), 180, 210, and 240 °C).

contrast, PTDPPTT, PTDPPBT, and PTDPPTVT exhibited higher carrier transport efficiency due to the edge-on backbone stacking structure. Note that the electrical properties of all four polymers changed after annealing. The detailed electrical property parameters of the films at different annealing temperatures are given in Figure 3b. The mobility of PTDPPSe gradually increased with the annealing temperature due to the high molecular weight and elevated side chain density of the polymer, ensuring film stability at high temperatures. In contrast, PTDPPTT, PTDPPBT, and PTDPPTVT exhibit cavities of various sizes in their films under high-temperature annealing due to their lower side chain density and entanglement than PTDPPSe, which disrupts the carrier transport paths. As a result, PTDPPSe exhibits increased mobility after annealing (Figure S4, Supporting Information), while PTDPPTT, PTDPPBT, and PTDPPTVT exhibit reduced mobility. The best electrical properties of PTDPPSe, PTDPPTT, PTDPPBT, and PTDPPTVT were obtained at temperatures of 240, 180, 180, and 180 °C, respectively. The average mobilities at these temperatures were estimated to be 1.30, 1.48, 1.69, and 1.30 cm^2 V^{-1} s^{-1}, respectively.

2.6. Stretching Properties of Polymer Films

The morphologies of stretched PTDPPSe, PTDPPTT, PTDPPBT, and PTDPPTVT films were investigated by stretching the films from 0–100% strain. The stretched films were prepared by the reported multiple transfer method shown in **Figure 4**a. OM and AFM images of the films were taken at different stretching

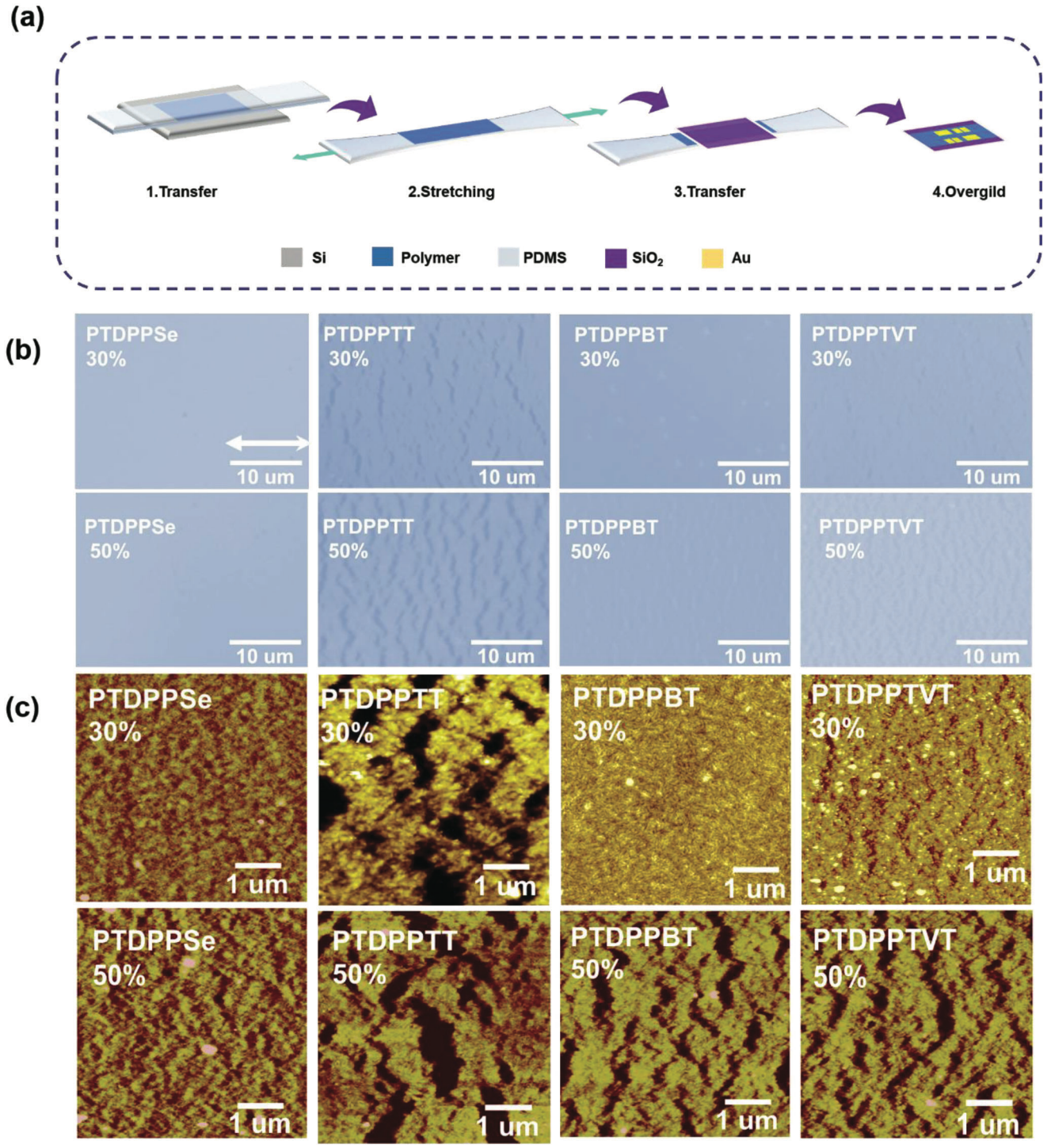

Figure 4. a) Flow chart of the devices preparation steps for the thin-film stretch tests. b) OM images of four polymer films at 30% and 50% stretching ratios. c) AFM images of four polymer films at 30% and 50% stretching ratios.

percentages, and the results are presented in Figure 4b,c and Figures S7, S8 (Supporting Information). PTDPPSe revealed only a slight amount of microcracking until 100% stretching ratio. This is resulted from the soft backbone and elevated molecular weight of PTDPPSe, leading to poor crystallinity and dense molecular chain entanglement. The movement of amorphous regions and molecular chains under the action of external forces provided stress dissipation and reduced cracking. PTDPPBT and PTDPPTVT films have a very similar morphology when stretched. Both start cracking at 50% strain. PTDPPTT has the worst tensile properties, showing significant cracking at 30% tensile ratio. Thus, the donor structure sub-

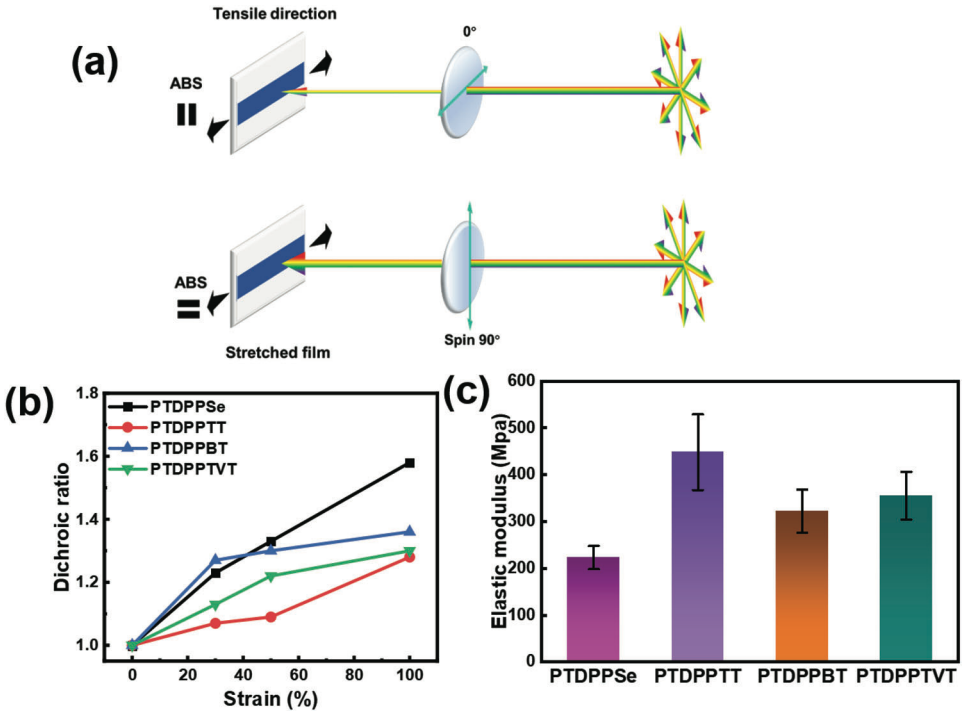

Figure 5. a) Schematic diagram of the dichroism test setup. b) Change in dichroic ratios under different strains for the four polymer films. c) Estimated elastic moduli of the four different polymers obtained from the FOE method.

stantially influenced the tensile morphologies of the polymer films.

To analyze the effect of stretching on the orientation of molecular chains inside the film, polarized UV–vis spectroscopy was used to investigate the alignment of crystalline and amorphous regions in the polymer films (**Figure 5**a).[7] The dichroic ratio was tested for each material after different stretching ratios (Figure 5b). The polymer molecular chains were oriented along the stretching direction during the stretching process, leading to an increased dichroic ratio. At 100% strain, the dichroic ratios of PTDPPSe, PTDPPTT, PTDPPBT, and PTDPPTVT films were estimated to be 1.58, 1.28, 1.36, and 1.30, respectively. The dichroic ratio greater than 1 would indicate all four conjugated polymers with obvious orientation. Consequently, PTDPPSe possessed the most pronounced molecular orientation upon stretching, followed by PTDPPBT polymer. In addition, the moduli of the semiconductor polymer films were measured indirectly by the film-on-elastomer (FOE) method.[41] In Figure 5c, the elastic moduli of PTDPPSe, PTDPPTT, PTDPPBT, and PTDPPTVT were recorded as 223 ± 25, 448 ± 81, 322 ± 46, and 355 ± 51 MPa, respectively. Detailed OM images of the FOE method are provided in Figure S9 (Supporting Information). The moduli of all four polymers appeared to be relatively low due to the high molecular weights of the polymers resulting from the elevated solubility of the silicone side chain-modified DPP acceptor.

To investigate the stretchable film properties, organic field-effect transistors were prepared. **Figure 6**b,c shows the trend of average mobilities of OFET devices prepared from stretched films at different stretching ratios. The average and max mobility values for stretching of the four polymers are summarized in Table S3 (Supporting Information). The changes in charge-carrier mobility as a function of strain, as well as the variations in normalized maximum current, are shown in Figure 6d,e. The electrical properties of PTDPPSe films remained stable after a slight decrease in the perpendicular to the stretching direction and gradually increased with the strain ratio in parallel to the stretching direction after stretching. After 100% strain, mobility in the perpendicular direction remained at 0.23 $cm^2\ V^{-1}\ s^{-1}$, equivalent to 46% of the initial level; the mobility in the parallel direction remained at 0.89 $cm^2\ V^{-1}\ s^{-1}$, equivalent to 1.65-fold higher than the initial film. This phenomenon has also been emerged and explained in our previous studies. The electrical anisotropy in the stretched film devices is caused by the high elasticity and dense entanglement of PTDPPSe.[19,42–44] The electrical properties of PTDPPBT and PTDPPTVT films exhibited an increasing trend after stretching and then decreased. PTDPPBT exhibited excellent carrier transport characteristics at 50% strain, with mobility of 2.37 $cm^2\ V^{-1}\ s^{-1}$ parallel to the stretched direction and 1.74 $cm^2\ V^{-1}\ s^{-1}$ perpendicular to the stretched direction. These values were 1.91 and 1.40-fold higher than those in the unstretched state. The mobilities of PTDPPTVT film at 50% strain were estimated to be 1.42 $cm^2\ V^{-1}\ s^{-1}$ in the parallel direction and 1.46 $cm^2\ V^{-1}\ s^{-1}$ in the perpendicular direction, equivalent to 1.12 and 1.15-fold those in unstretched films.[45–47] For PTDPPTT, the mobility parallel to the tensile direction increases slightly at 30% strain and then decreases rapidly, while the mobility perpendicular to the tensile direction decreases monotonously with the increase of strain.

Figure 7a summarizes the structure and performance parameters of the four conjugated polymers with different donors. It can be seen that the electrical properties of the four polymers are positively correlated with aggregation and crystallinity, and

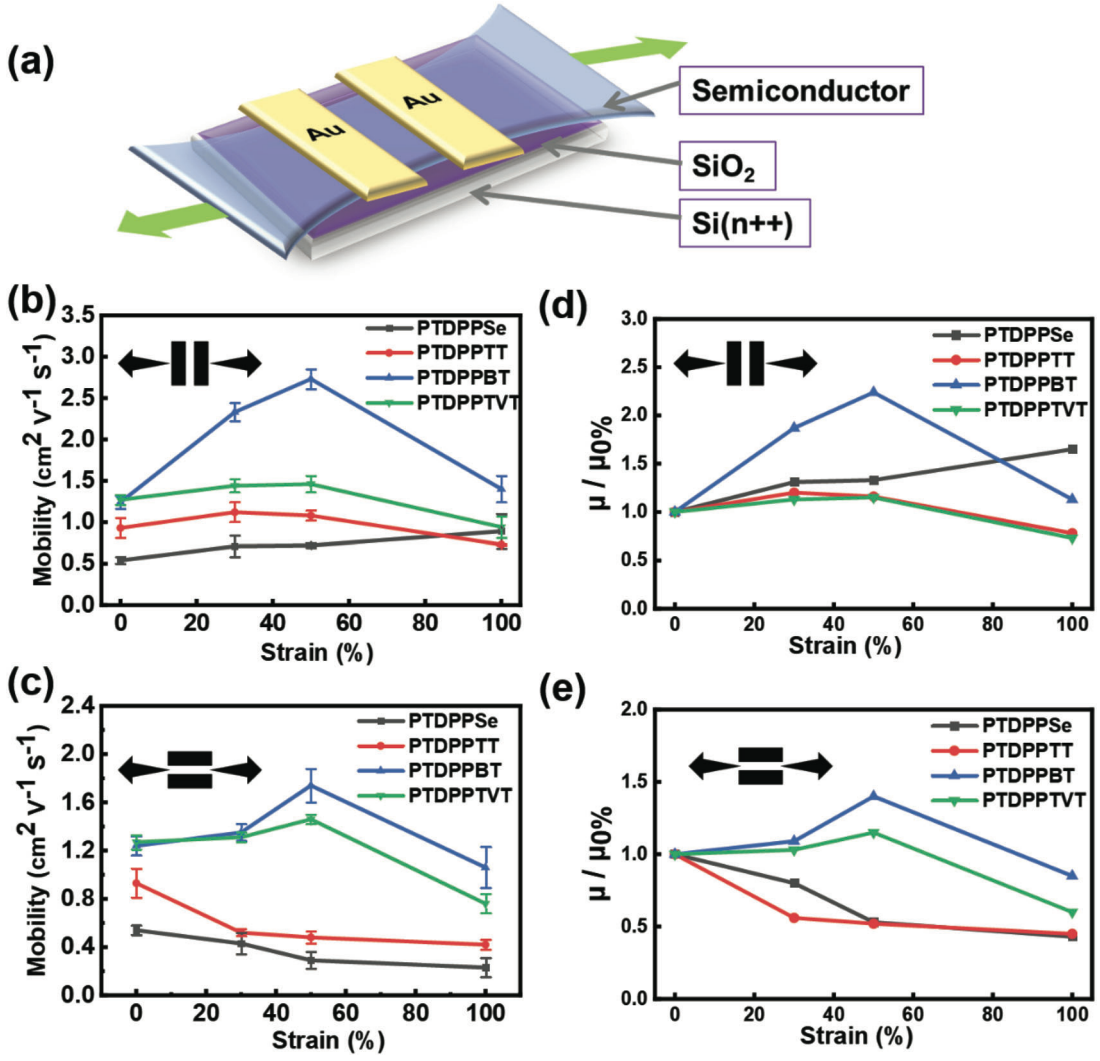

Figure 6. a) Architecture of OFETs stretched polymer thin films. b,c) Charge mobilities of the polymer thin films under different strains in parallel and perpendicular to the strain direction. d,e) μ/μ_0 of the four polymer materials under different perpendicular and parallel stretching ratios.

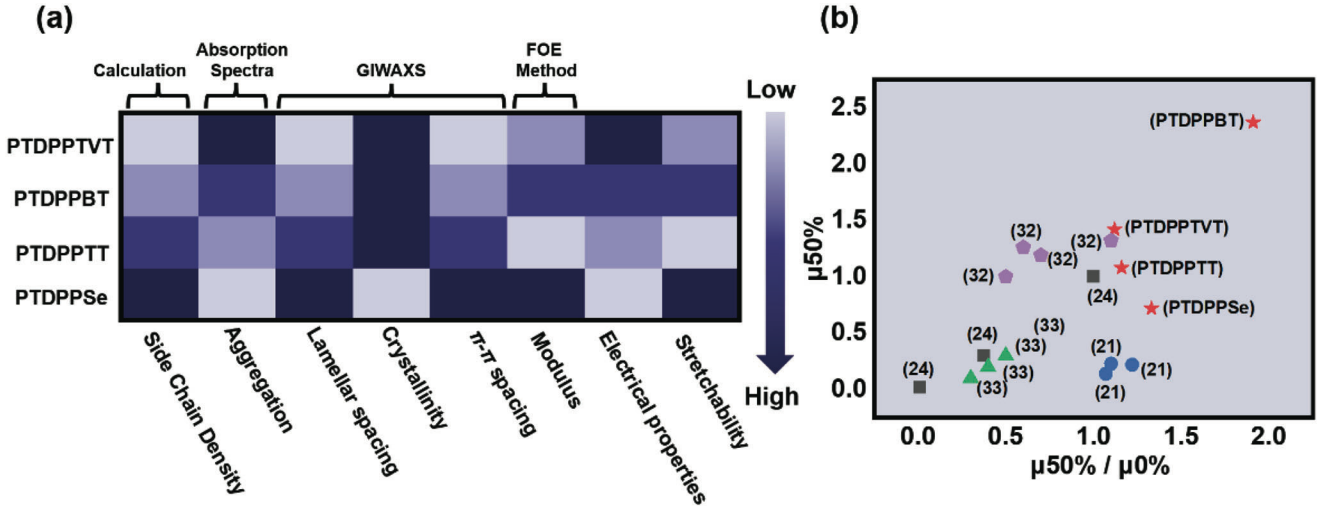

Figure 7. a) Summary of various factors affecting the charge mobilities and stretchability of four polymers. b) The ratio of mobility at 50% strain to mobility at 0% strain for the four polymers in this study compared with stretchable polymer semiconductors reported in the literature.

negatively correlated with side chain density, lamellar spacing, and π–π stacking distance. With some exceptions for PTDPPTT, the stretchable properties of the conjugated polymers showed an opposite trend to the electrical properties. This suggests that increasing the conjugate length of the donor unit, especially using a fused structure such as TT, leads to an increase in the elastic modulus and a decrease in the stretchable properties, which is consistent with the results reported in the literature.[29] It is worth noting that the use of BT as the donor can significantly improve the electrical properties of the material while maintaining moderate stretchability. It has much higher mobility at 50% strain than most of the reported stretchable conjugated polymers (Figure 7b).

3. Conclusion

The effects of donor structures on the charge transport properties and mechanical properties of DPP-based D–A polymers modified with siloxane side chains were systematically investigated. A series of polymers were obtained by the copolymerization of four donor species, selenophene (Se), thienothiophene (TT), bithiophene (BT), and thienylenevinylenethiophene (TVT), with siloxane side chain modified DPP acceptor. All four polymers showed high molecular weights due to the excellent solubilization of siloxane side chains. The donor structure affected the side chain density and intermolecular interactions, thereby impacting the stacking of the polymer in the solution and film states. For stacking and crystallinity of molecular chains, PTDPPSe adopts face-on orientation with poor crystallinity and the most significant layer spacing and π–π stacking distance. As a result, the polymer with selenophene as a donor displayed the worst electrical properties, but the soft molecular chains yielded the best stretchability. PTDPPTT, PTDPPBT, and PTDPPTVT are mainly edge-on staked and have higher crystallinity, leading to significantly enhanced electrical properties. Remarkably, PTDPPBT film showed a crack-onset-strain ≈50% strain, and mobility up to 2.37 $cm^2\ V^{-1}\ s^{-1}$ in the direction parallel to stretch at 50% strain, which is 1.91-fold higher than that of the unstretched film. Therefore, among the four donors studied, the combination of bithiophene and siloxane-modified DPP leads to conjugated polymer with excellent electrical and moderate stretchability which have promising applications in the development of wearable electronic devices.

4. Experimental Section

Materials: The chemical solvents and reagents used in this study were all purchased from Sinopharm Chemical Reagent Co., Ltd., Sigma-Aldrich, or Alfa Aesar. All reagents were used as received without further purification. 3,6-bis(5-bromothiophen-2-yl)-2,5-bis(7-(1,1,3,3,5,7,7,7-octamethyl-5-((trimethylsilyl)oxy)tetrasiloxane heptyl)-2,5 dihydropyrrolo (3,4-c) pyrrole-1,4-dione (DPP) was synthesized by previously reported methods. Each step of the synthesis process of the polymer PTDPPX is shown in Supporting Information. The accuracy of each step of the monomer was confirmed using NMR spectroscopy at 600 MH on an Agilent VNMRS600. The average molecular weight (M_n), weight average molecular weight (M_w), and polydispersity index (PDI) of four polymers were tested by Waters 1515 equipment with chloroform as the eluent at 25 °C.

Characterization: The UV–vis spectroscopy of the four polymers in solution and film states was tested by an Agilent Cali5000 UV–vis–NIR spectrophotometer instrument. Four polymer solutions were deposited on CYTOP-modified SiO_2 substrates, and the film morphology was investigated by SPA300HV AFM at different annealing temperatures and stretching ratios. The GIWAXS data for thin films deposited on silicon substrates were evaluated by a laboratory beamline system (Xenocs Inc. Xeuss 2.0). The X-ray wavelength was set to 1.54 Å, the distance from the film to the detector was 15 cm, and the angle of incidence was 0.2°. The films were tested in a vacuum environment to reduce air scattering. The modulus was calculated by the film-on-elastomer method according to Equation (1):

$$\frac{E_f}{1-\nu_f^2} = \frac{3E_s}{1-\nu_s^2}\left(\frac{\lambda}{2\pi d}\right)^3 \tag{1}$$

where E_s and E_f are the elastic moduli of polydimethylsiloxane (PDMS) substrate and polymer films, respectively. V_s and V_f refer to the Poisson ratios of the PDMS substrate and polymer films, respectively. λ is the buckling wavelength, and d_f denotes the thickness of four polymer films.

Preparation of Thin Film Transistor Devices: To study the charge transport properties of polymers, OFET devices with BGTC structure were prepared. The thickness of SiO_2 used as the dielectric layer was 300 nm, and the modified layer CYTOP was spin-coated on the SiO_2 surface at 3000 rpm. The devices were then placed in a vacuum glove box for annealing at different temperatures (RT, 180, 210, and 240 °C) before placing on a mask of 100 µm in length (L) and 1000 µm in width (W) to deposit, 40 nm gold in the coater as the source-drain. The electrical characteristics of OFETs were measured on a Keithley 4200 semiconductor parameter analyzer, and the mobility of each device in saturation was calculated by Equation (2):

$$I_{DS}\,(\text{sat}) = \frac{W}{2L}Ci \cdot \mu s_{at} \cdot (V_G - V_{th})^2 \tag{2}$$

where I_{DS} expresses the drain current in saturation, W/L is the channel width/length proportion, C_i donates the dielectric layer capacitance per unit area, and V_G and V_{th} are the gate and threshold voltages, respectively.

Preparation of Stretched Film Devices: A simple method was used to transfer the films multiple times to study the surface morphologies and carrier transport properties of the conjugated polymers at different stretching ratios. The adhesion properties of cross-linked PDMS were employed to transfer the film to PDMS. The polymer/PDMS was subsequently stretched to a specific strain (0%, 30%, 50%, and 100%) followed by transfer of the stretched film to a CYTOP-modified SiO_2/Si substrate. Finally, the BGTC OFET devices were fabricated by thermal evaporation of the upper source-drain electrodes through the use of a metal mask (length = 100 µm, width = 1000 µm).

Supporting Information

Supporting Information is available from the Wiley Online Library or from the author.

Acknowledgements

N.W. and G.H. contributed equally to this work. This study was supported by the National Natural Science Foundation of China (NSFC, grant no. 52273172, 62274053), the National Key Research and Development Program of China (2022YFE0198200), the Major Science and Technology Project of Anhui Province (2021e03020007), and the Natural Science Foundation of Hefei (2022031, 2022002). X.G. and Y.W. thank National Science Foundation for providing funding resources for the mechanical property measurement under award number DMR-2047689.

Conflict of Interest

The authors declare no conflict of interest.

Data Availability Statement

The data that support the findings of this study are available on request from the corresponding author. The data are not publicly available due to privacy or ethical restrictions.

Keywords

backbone engineering, donor structures, D-A conjugated polymers, electrical properties, mechanical properties

Received: March 23, 2023
Revised: April 25, 2023
Published online:

[1] I. You, D. G. Mackanic, N. Matsuhisa, J. Kang, J. Kwon, L. Beker, J. Mun, W. Suh, T. Y. Kim, J. B.-H. Tok, Z. Bao, U. Jeong, *Science* **2020**, *370*, 961.
[2] Y. Liu, M. Pharr, G. A. Salvatore, *ACS Nano* **2017**, *11*, 9614.
[3] X. Yu, L. Chen, C. Li, C. Gao, X. Xue, X. Zhang, G. Zhang, D. Zhang, *Adv. Mater.* **2023**, *35*, 2209896.
[4] K. Müllen, W. Pisula, *J. Am. Chem. Soc.* **2015**, *137*, 9503.
[5] Y.u Zheng, S. Zhang, J. B.-H. Tok, Z. Bao, *J. Am. Chem. Soc.* **2022**, *144*, 4699.
[6] B. Roth, S. Savagatrup, N. V. De Los Santos, O. Hagemann, J. E. Carlé, M. Helgesen, F. Livi, E. Bundgaard, R. R. Søndergaard, F. C. Krebs, D. J. Lipomi, *Chem. Mater.* **2016**, *28*, 2363.
[7] Y. Zheng, G. J. N. Wang, J. Kang, M. Nikolka, H. C. Wu, H. Tran, S. Zhang, H. Yan, H. Chen, P. Y. Yuen, J. Mun, R. H. Dauskardt, I. McCulloch, J. B. H. Tok, X. Gu, Z. Bao, *Adv. Funct. Mater.* **2019**, *29*, 3697.
[8] Y. Zhao, X. Zhao, Y. Zang, C.-A. Di, Y. Diao, J. Mei, *Macromolecules* **2015**, *48*, 2048.
[9] Y. Zhao, X. Zhao, M. Roders, A. Gumyusenge, A. L. Ayzner, J. Mei, *Adv. Mater.* **2017**, *29*, No.
[10] X. Zhao, Y. Zhao, Q. Ge, K. Butrouna, Y. Diao, K. R. Graham, J. Mei, *Macromolecules* **2016**, *49*, 2601.
[11] D. H. Ho, R. Song, Q. Sun, W.-H. Park, S. Y. Kim, C. Pang, D. H. Kim, S.-Y. Kim, J. Lee, J. H. Cho, *ACS Appl. Mater. Interfaces* **2017**, *9*, 44678.
[12] H. Tran, V. R. Feig, K. Liu, H.-C. Wu, R. Chen, J. Xu, K. Deisseroth, Z. Bao, *ACS Cent. Sci.* **2019**, *5*, 1884.
[13] D. C. Kim, H. J. Shim, W. Lee, J. H. Koo, D.-H. Kim, *Adv. Mater.* **2020**, *32*, 1902743.
[14] R. Yuan, W. Qian, Z. Liu, J. Wang, J. Xu, K. Chen, L. Yu, *Small* **2022**, *18*, e2104690.
[15] D. Choi, H. Kim, N. Persson, P.-H. Chu, M. Chang, J.-H. Kang, S. Graham, E. Reichmanis, *Chem. Mater.* **2016**, *28*, 1196.
[16] Y.-C. Lin, Y.-W. Huang, C.-C. Hung, Y.-C. Chiang, C.-K. Chen, L.-C. Hsu, C.-C. Chueh, W.-C. Chen, *ACS Appl. Mater. Interfaces* **2020**, *12*, 50648.
[17] J. Y. Oh, S. Rondeau-Gagné, Y.-C. Chiu, A. Chortos, F. Lissel, G.-J. N. Wang, B. C. Schroeder, T. Kurosawa, J. Lopez, T. Katsumata, J. Xu, C. Zhu, X. Gu, W.-G. Bae, Y. Kim, L. Jin, J. W. Chung, J. B.-H. Tok, Z. Bao, *Nature* **2016**, *539*, 411.
[18] H.-C. Wu, F. Lissel, G.-J. N. Wang, D. M. Koshy, S. Nikzad, H. Yan, J. Xu, S. Luo, N. Matsuhisa, Y. Cheng, F. Wang, B. Ji, D. Li, W.-C. Chen, G. Xue, Z. Bao, *Adv. Funct. Mater.* **2021**, *31*, 2009201.
[19] J. Mun, Y. Ochiai, W. Wang, Y. Zheng, Y.-Q. Zheng, H.-C. Wu, N. Matsuhisa, T. Higashihara, J. B.-H. Tok, Y. Yun, Z. Bao, *Nat. Commun.* **2021**, *12*, 3572.
[20] Y. Ding, Y. Zhu, X. Wang, Y. Wang, S. Zhang, G. Zhang, X. Gu, L. Qiu, *Chem. Mater.* **2022**, *34*, 2696.
[21] Y. Ding, Y. Yuan, N. Wu, X. Wang, G. Zhang, L. Qiu, *Macromolecules* **2021**, *54*, 8849.
[22] F. Zhao, Y. Yuan, Y. Ding, Y. Wang, X. Wang, G. Zhang, X. Gu, L. Qiu, *Macromolecules* **2021**, *54*, 5440.
[23] G. Huang, N. Wu, X. Wang, G. Zhang, L. Qiu, *Macromol. Rapid. Commun.* **2022**, *43*, 2200149.
[24] D. Pei, Z. Wang, Z. Peng, J. Zhang, Y. Deng, Y. Han, L. Ye, Y. Geng, *Macromolecules* **2020**, *53*, 4490.
[25] T. Lei, J.-H. Dou, X.-Y. Cao, J.-Y. Wang, J. Pei, *J. Am. Chem. Soc.* **2013**, *135*, 12168.
[26] G.-J. N. Wang, L. Shaw, J. Xu, T. Kurosawa, B. C. Schroeder, J. Y. Oh, S. J. Benight, Z. Bao, *Adv. Funct. Mater.* **2016**, *26*, 7254.
[27] Y.-W. Huang, Y.-C. Lin, H.-C. Yen, C.-K. Chen, W.-Y. Lee, W.-C. Chen, C.-C. Chueh, *Chem. Mater.* **2020**, *32*, 7370.
[28] M. U. Ocheje, M. Selivanova, S. Zhang, T. H. Van Nguyen, B. P. Charron, C.-H. Chuang, Y.-H. Cheng, B. Billet, S. Noori, Y.-C. Chiu, X. Gu, S. Rondeau-Gagné, *Polym. Chem.* **2018**, *9*, 5531.
[29] S. Zhang, M. U. Ocheje, L. Huang, L. Galuska, Z. Cao, S. Luo, Y.-H. Cheng, D. Ehlenberg, R. B. Goodman, D. Zhou, Y. Liu, Y.-C. Chiu, J. D. Azoulay, S. Rondeau-Gagné, X. Gu, *Adv. Electron. Mater.* **2019**, *5*, 1800899.
[30] J. Mun, G. J. N. Wang, J. Y. Oh, T. Katsumata, F. L. Lee, J. Kang, H. C. Wu, F. Lissel, S. Rondeau-Gagné, J. B. H. Tok, Z. Bao, *Materials* **2018**, *28*, 1804222.
[31] D. Liu, J. Mun, G. Chen, N. J. Schuster, W. Wang, Y. Zheng, S. Nikzad, J.-C. Lai, Y. Wu, D. Zhong, Y. Lin, Y. Lei, Y. Chen, S. Gam, J. W. Chung, Y. Yun, J. B.-H. Tok, Z. Bao, *J. Am. Chem. Soc.* **2021**, *143*, 11679.
[32] S. Tu, T. Tian, A. Lena Oechsle, S. Yin, X. Jiang, W. Cao, N. Li, M. A. Scheel, L. K. Reb, S. Hou, A. S. Bandarenka, M. Schwartzkopf, S. V. Roth, P. Müller-Buschbaum, *Chem. Eng. J.* **2022**, *429*, 132295.
[33] K. Huang, G. Huang, X. Wang, H. Lu, G. Zhang, L. Qiu, *ACS Appl. Mater. Interfaces* **2020**, *12*, 17790.
[34] S.-H. Kang, D. Lee, W. Choi, J. H. Oh, C. Yang, *Macromolecules* **2022**, *55*, 4367.
[35] X. Jiang, Y. Xu, X. Wang, Y. Wu, G. Feng, C. Li, W. Ma, W. Li, *Phys. Chem. Chem. Phys.* **2017**, *19*, 8069.
[36] L. Collins, Y. Liu, O. S. Ovchinnikova, R. Proksch, *ACS Nano* **2019**, *13*, 8055.
[37] Z.-F. Yao, Z.-Y. Wang, H.-T. Wu, Y. Lu, Q.-Y. Li, L. Zou, J.-Y. Wang, J. Pei, *Angew. Chem., Int. Ed.* **2020**, *59*, 17467.
[38] S. Park, M. H. Lee, K. S. Ahn, H. H. Choi, J. Shin, J. Xu, J. Mei, K. Cho, Z. Bao, D. R. Lee, M. S. Kang, D. H. Kim, *Adv. Funct. Mater.* **2016**, *26*, 4627.
[39] T. Lei, X. Xia, J.-Y. Wang, C.-J. Liu, J. Pei, *J. Am. Chem. Soc.* **2014**, *136*, 2135;
[40] T. Wang, A. D. F. Dunbar, P. A. Staniec, A. J. Pearson, P. E. Hopkinson, J. E. Macdonald, S. Lilliu, C. Pizzey, N. J. Terrill, A. M. Donald, A. J. Ryan, R. A. L. Jones, D. G. Lidzey, *Soft Matter* **2010**, *6*, 4128.
[41] E. L. Melenbrink, K. M. Hilby, M. A. Alkhadra, S. Samal, D. J. Lipomi, B. C. Thompson, *ACS Appl. Mater. Interfaces* **2018**, *10*, 32426.
[42] J.-H. Kim, A. Nizami, Y. Hwangbo, B. Jang, H.-J. Lee, C.-S. Woo, S. Hyun, T.-S. Kim, *Nat. Commun.* **2013**, *4*, 2520.
[43] J. Choi, W. Kim, D. Kim, S. Kim, J. Chae, S. Q. Choi, F. S. Kim, T.-S. Kim, B. J. Kim, *Chem. Mater.* **2019**, *31*, 3163.
[44] S. Zhang, Y. H. Cheng, L. Galuska, A. Roy, M. Lorenz, B. Chen, S. Luo, Y. T. Li, C. C. Hung, Z. Qian, P. B. J. St. Onge, G. T. Mason, L. Cowen, D. Zhou, S. I. Nazarenko, R. F. Storey, B. C. Schroeder, S. Rondeau-Gagné, Y. C. Chiu, X. Gu, *Adv. Funct. Mater.* **2020**, *30*, 2000663.
[45] A. X. Chen, A. T. Kleinschmidt, K. Choudhary, D. J. Lipomi, *Chem. Mater.* **2020**, *32*, 7582.
[46] G. Zhang, S. Lee, E. Gutiérrez-Meza, C. Buckley, M. Mcbride, D. A. Valverde-Chávez, Y. H. Kwon, V. Savikhin, H. Xiong, T. J. Dunn, M. F. Toney, Z. Yuan, C. Silva, E. Reichmanis, *Chem. Mater.* **2019**, *31*, 6530.
[47] Y.e Yuan, F. Zhao, Y. Ding, G. Zhang, X. Wang, L. Qiu, *Macromol. Rapid. Commun.* **2022**, *43*, 2100636.

